Nuclear Instruments and Methods in Physics Research A 713 (2013) 11–18

Contents lists available at SciVerse ScienceDirect

Nuclear Instruments and Methods in Physics Research A

journal homepage: www.elsevier.com/locate/nima

Influence of the interstrip gap on the response and the efficiency of Double Sided Silicon Strip Detectors

D. Torresi [a,b,*], D. Stanko [c], A. Di Pietro [a], P. Figuera [a], M. Fisichella [a,d], M. Lattuada [a,e], M. Milin [c], A. Musumarra [a], M. Pellegriti [a], V. Scuderi [a], E. Strano [a,e], M. Zadro [f]

[a] INFN, Laboratori Nazionali del Sud, Catania, Italy
[b] Centro Siciliano di Fisica Nucleare e Struttura della Materia, Catania, Italy
[c] University of Zagreb, Zagreb, Croatia
[d] Universitá di Messina, Messina, Italy
[e] Universitá degli studi di Catania, Dipartimento di Fisica e Astronomia, Catania, Italy
[f] Ruđer Bošković Institute, Zagreb, Croatia

ARTICLE INFO

Article history:
Received 6 November 2012
Received in revised form
16 February 2013
Accepted 22 February 2013
Available online 5 March 2013

Keywords:
DSSSD
Interstrip
Efficiency

ABSTRACT

Double Sided Silicon Strip Detectors (DSSSD) are highly segmented detectors that are widely used in nuclear physics especially in radioactive beam experiments where, due to the low beam intensities, one needs to cover large solid angles with high granularity. A study of the response of DSSSDs, using ^{7}Li and ^{16}O beams at different energies is presented. In order to characterize the detector behavior for events corresponding to particles entering the detector in the interstrip gap both for ohmic and junction sides, signals of positive and negative polarities were acquired at the same time. Different procedures for the selection of full energy events and for the determination of the corresponding efficiencies are shown and discussed.

1. Introduction

Highly segmented silicon detectors has became of standard use in nuclear physics either in structure and nuclear dynamics studies. Their segmentations are very useful for studying angular distributions of various processes such as elastic scattering, transfer, break-up, etc., see e.g. Refs. [1–4], or to study reactions where coincidences between two or more particles are requested to fully characterize the final state [5,6]. They are also used in experiments where the cluster structure of stable and unstable nuclei is investigated by using the inverse kinematic thick target scattering method, e.g. Refs. [7,8], that allows to measure the elastic scattering excitation function by using a single beam energy. Again large solid angles are very useful when unstable beams are used in order to have high geometric efficiency with good granularity, e.g. Refs. [9,10]. Double Sided Silicon Strip Detectors (DSSSD) can also be used as active stoppers to measure for example the β decay time of exotic nuclei produced by fragmentation. The fragments are implanted on the DSSSDs and detected together with the subsequent β decay; these events are then correlated on a pixel-by-pixel basis, e.g. Refs. [11–13].

DSSSDs have both sides segmented and are commercially available with a wide choice of shapes and thicknesses. Indicating as N_f and N_b the number of strips on the front (junction) and back (ohmic) sides, respectively, these detectors allow to have information on $N_f \times N_b$ pixels (overlap regions between front and back strips) by using just $N_f + N_b$ electronic channels. The segmentation of silicon strip detectors is obtained by means of a SiO_2 insulating layer interposed between adjacent strips. The presence of the insulating layer affects the charge collection on each strip for particles whose trajectory crosses an interstrip region. It is known from the literature [14–17] that particles impinging onto the detector through an interstrip give rise to signals, in the two adjacent strips separated by the interstrip region under consideration, with an amplitude which is smaller than the full energy one. Moreover, for front interstrip events, one can also have the presence of signals with inverse polarity [14–17]. For this reason, when analyzing data collected by using DSSSDs, it is very important to be able to select events that produce signals with the correct full energy amplitude and to reject interstrip events producing signals of amplitude smaller than the full energy one. The ratio between the number of events detected with the full energy and the total number of events will be called in the following *efficiency for full energy detection*. Such an efficiency is

* Corresponding author at: INFN, Laboratori Nazionali del Sud, Catania, Italy. Tel.: +39 0498275913.
E-mail addresses: torresi@lns.infn.it, torresi@pd.infn.it (D. Torresi).

0168-9002/$ - see front matter © 2013 Elsevier B.V. All rights reserved.
http://dx.doi.org/10.1016/j.nima.2013.02.027

therefore lower than 100%, as it can be expected for single pad silicon detectors, and its knowledge is crucial in those experiments where absolute cross-sections have to be extracted. The aim of the present study is to determine the efficiency for the full energy detection, to characterize the interstrip behavior and to investigate the possibility to reconstruct the energy of the particles impinging on the interstrip. Studies on the interstrip effects were done by using for example α-particles of low energy [14,15], 3 MeV protons [15], 59.5 keV γ rays from ^{241}Am [16] and laser beams with wavelength of 660 and 1060 nm [17]. We performed, for the first time, a systematic study irradiating detectors with ^{7}Li and ^{16}O beams in the energy range 6–50 MeV.

The paper is organized in the following way. Section 2 gives the descriptions of the tested detectors and the experimental set-up. In Section 3 the response of these detectors will be presented. Section 4 gives a discussion of the results. In Section 5 we will discuss on possible procedures for full energy selection and the associated efficiency. Finally, in Section 6, the obtained results will be summarized.

2. Experimental set-up

The DSSSDs under investigation in the present study are Micron Semiconductor Ltd. model W1, 1000 and 500 μm thick. They have an active area of 50×50 mm^2 and each side is divided into 16 parallel strips. The strips on the junction side (front) are perpendicular to the ones on the ohmic side (back), giving a granularity of 256 square shaped pixels. Each strip is 3 mm wide and 50 mm long, and is insulated by a 0.1 mm wide and 1 μm thick silicon dioxide layer (interstrip). The metalization is made of a 3000 Å thick Al layer, and a silicon dead layer of 0.5 μm thick is also present. The full depletion voltage of the detectors is around 200 V.

The experiment was performed by sending ^{7}Li and ^{16}O beams, delivered by the SMP Tandem of Laboratori Nazionali del Sud in Catania, on the three DSSSDs. Two of them had a thickness of 1000 μm and were irradiated from the front (junction) side. The third one had a thickness of 500 μm and was irradiated from the back (ohmic) side. The detectors were placed on a rotating platform inside the CT2000 scattering chamber, allowing to place each of them at zero degree**s** with respect to the beam direction.

Table 1
Calculated range in Si for the ^{7}Li and ^{16}O beam energies used in the present work.

^{7}Li energy (MeV)	29.7	23.6	19.6	16.5	14.5	12.4	11.5	10.5
Range in Si (μm)	130	91	68	53	44	36	31.9	28.1
^{16}O energy (MeV)	49.6	45.5	39.4	32.1	23.8	15.5	6.0	
Range in Si (μm)	37	33	28	22	15	10	4	

Beams with a reduced intensity of the order of 100 pps were directly sent onto each detector.

The electronics was assembled in such a way that it was possible to measure the signals of both polarities at the same time. In fact normal signals coming from the junction side are positive, whereas the ones coming from the ohmic side are negative. However, as already discussed in Refs. [14–17], anomalous signals with inverse polarity are present for particles entering the detector in proximity of an interstrip region. In order to acquire at the same time the signals of both polarities for all strips, the signals coming out from the preamplifiers (both for junction and ohmic side) were passively split into two equal signals. These twin signals were sent to programmable amplifiers where only the polarity of one of them was inverted. Finally, after amplification, they were sent to a peak sensing ADC that was able to convert only positive signals. In this way we were able to measure, at the same time, the signals of both polarities. In order to study the dependence of the interstrip effects on the implantation depth, the ^{7}Li and ^{16}O beams were used with different energies, as listed in Table 1.

The used beams were characterized by a broad profile (about 1×1 cm^2) and very low intensity (around 100 pps). For each energy we repeated the measurements for two different polarization voltages corresponding to 1 Full Depletion Voltage (FDV) and 1.4 FDV, in order to study the change of the response of the detector with the applied bias.

3. DSSSDs phenomenology

Typical energy spectra for a single front and a single back strips using a ^{7}Li beam at 14.5 MeV are shown in Fig. 1. The peak on the right is the full energy peak (FEP), corresponding to particles entering the detector through a strip. The typical FWHM of this peak (that is the resolution of the detector) is around 110 keV both for front and back sides. The peak on the left is the pedestal corresponding to events with zero energy. This is due to particles that trigger the acquisition hitting other strips, without producing a signal in the strip considered in the figure. The main features in Fig. 1 are the following.

(a) The "continuum" of events with energy in between the two main peaks. As it will be shown in the following, such events are due to particles whose trajectory crosses the interstrip region and will be named *interstrip events*.

(b) The presence of anomalous signals with opposite polarity (i.e. events with "negative energy" in the figure) in the front strip spectra. Very few opposite polarity signals, without any correlations with adjacent strips are observed in back strip spectra.

The presence of opposite polarity signals, in the front side, was already observed in Refs. [14–17] and it will be discussed in more detail in the following. In Fig. 2 it is shown the fraction of events

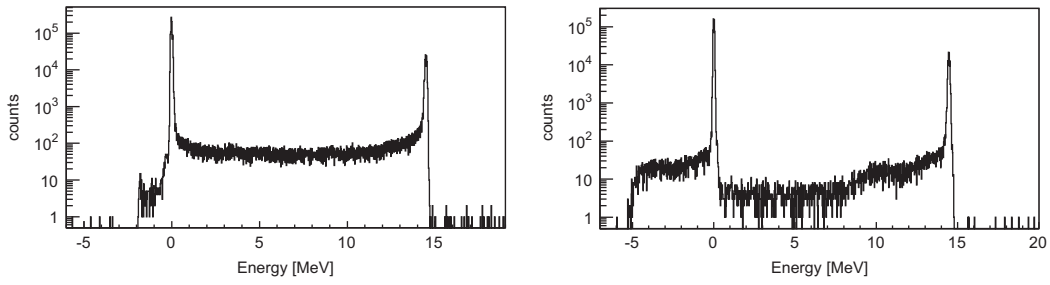

Fig. 1. Typical energy spectra from back (left panel) and front strips (right panel) observed irradiating the detector with monoenergetic ^{7}Li ions at 14.5 MeV. In both figures the peak on the right is the full energy peak, whereas the left peak is the pedestal. Pulses with negative polarity corresponding to "negative energy" events are clearly present in the front strips energy spectrum. See text for further details.

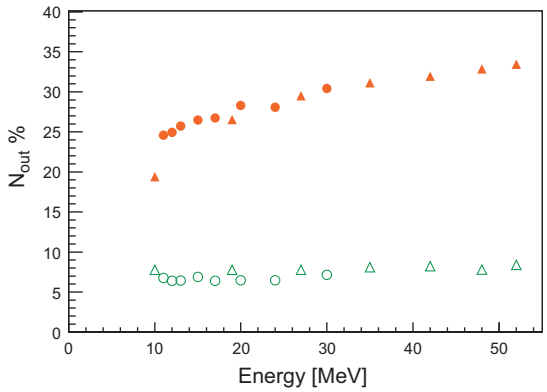

Fig. 2. Fraction of events out of the FEP (3σ) as a function of the incoming energy for the ^{7}Li (circles) and ^{16}O beams (triangles) for a bias of 1 FDV. Open symbols refer to the front side whereas full symbols refer to the back side.

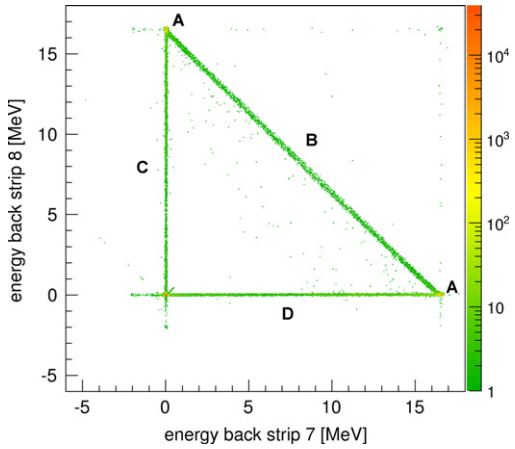

Fig. 3. Energy correlation between two adjacent back strips using a ^{7}Li beam at an energy of 16.5 MeV. The different regions labeled *A B C D* are described in the text.

with energy lower than the FEP (both positive and negative polarity signals) with respect to the total number of events for back and front strips and for particles of different energies. Although the pure geometrical size of the interstrip is the same for front and back strips, the fraction of back interstrip events is systematically larger than one of the front interstrip. Moreover, such a fraction depends on the energy of the incident particles.

3.1. Adjacent strip correlations

In Fig. 3 the coincidence plot between two adjacent back strips is shown. The regions labeled *A* correspond to particles entering the detector through a strip and giving rise to a full energy signal. The interstrip events (those with energy lower than FEP) are seen as a coincidence between two adjacent strips (labeled *B*) since the charge generated in the detector is collected by both strips. Such type of coincidences were not observed between strips which are not adjacent, with the exception of the two strips at the edge of the detector (1st and 16th) occasionally in coincidence with a third strip. These events are probably produced by particles entering the detector in the region between the edge of one strip and the guard ring that surrounds the active surface of the detector. We underline that by summing the charge collected by the two adjacent strips in coincidence, one obtains the full energy of the incident particles. In other words, the interstrip events on the back side are characterized by an asymmetric sharing of the charge between the two adjacent strips without any loss of charge. Therefore, by summing the two signals, one can correctly reconstruct the full energy. We note that the region *C* corresponds to interstrip events between back strips 8 and 9, whereas region *D* corresponds to interstrip events between back strips 7 and 6.

The coincidence plot of two adjacent front strips has a more complicated pattern as it is shown in Fig. 4. The regions labeled *A* correspond again to particles entering the detector through a strip which collects all charges generating a full energy signal. The interstrip region is not a simple straight line joining the two full energy regions *A*, as observed for the back strips. In fact, there are two classes of events: in the first class both adjacent strips produce positive signals (region labeled *B*), in the second class one of the two signals has an anomalous polarity corresponding to "negative energy" in the spectrum (regions labeled *C*).

Fig. 5 shows the fraction of interstrip events (including both front and back interstrips) as a function of the incident energy for the two different bias values and for the two beams. In this case, interstrip events are counted as events where it is present a coincidence of signals of any polarity in two adjacent strips. The amount of random coincidences, due to beam particles reaching the detector within the same acquisition gate, is negligible since the beam intensity is less than 100 pps. It is important to notice the difference with respect to Fig. 2 where, for each 1D energy spectrum, we integrated the number of events under the FEP without taking into account any correlation. As one can see from Fig. 5, the measured fraction of interstrip events is significantly larger than the one expected from pure geometrical

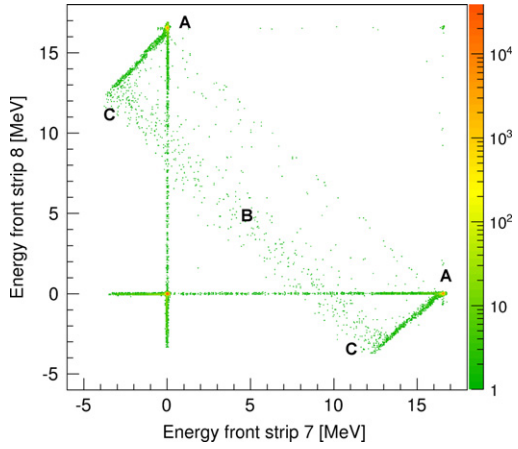

Fig. 4. Energy correlations between two adjacent front strips using a ^{7}Li beam at an energy of 16.5 MeV. The different regions labeled *A B C* are described in the text.

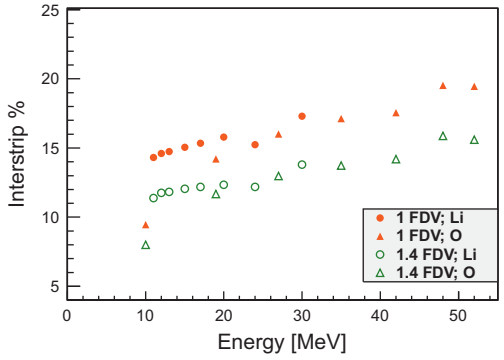

Fig. 5. Fraction of interstrip events with respect to the total number of events, calculated as coincidence events on two adjacent strips for ^{7}Li (circles) and ^{16}O beams (triangles). Full symbols refer to a bias of 1 FDV whereas empty symbols refer to 1.4 FDV.

considerations which would be of the order of 6.2% (i.e. 3.1% for each side of the detector). Differences between the effective width and the geometrical width of the interstrip area were already observed in Ref. [18]. Furthermore Fig. 5 shows that the number of interstrip events increases with the energy and depends on the applied bias. Another effect of the applied bias concerns with the amplitude of the negative signals for the front interstrip events, which is lower when a 1.4 FDV is applied to the detector. This will be described in more detail in the next subsection.

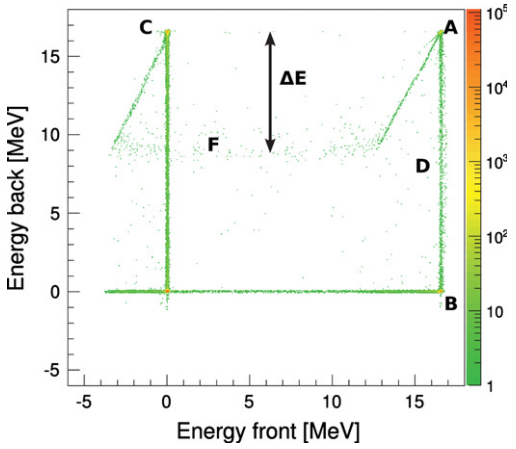

Fig. 6. Energy correlations between back strip 8 and front strips 7 and 8. The different regions labeled *A B C D F ΔE* are described in the text.

3.2. Front-side back-side correlations

In order to better understand the behavior of such interstrip events as a function of the incident energy and applied bias, it is useful to look at the front–back correlation plots. A typical plot of this kind is shown in Fig. 6. Here the correlation between the energy deposited into front strips 7 and 8 (*x*-axis) with the corresponding energy deposited into the back strip 8 (*y*-axis) is shown. The region labeled *A* corresponds to particles entering the detector through the front strip 7 or 8 and through the back strip 8 (i.e. full energy on both sides). The region labeled *C* corresponds to particles that hit back strip 8 and a front strip different than strip 7 or 8, so that the full energy is observed only in the *y*-axis whereas zero energy is observed in the *x*-axis. The region labeled *B* corresponds to all those particles entering the detectors through the strip front 7 or 8 and hitting a back strip different from strip 8, thus the full energy is observed only in a front strip whereas zero energy is observed in the *y*-axis. In the region labeled *D* the full energy for front strip 7 or 8 is observed whereas a lower energy for the back is observed: these are back interstrip events. The region labeled *F* shows that front interstrip events affect also the back signals; in fact, in the presence of a front interstrip event the signal generated in the back is lower than the full energy. In this case back strip events suffer a sort of "energy defect" due to the

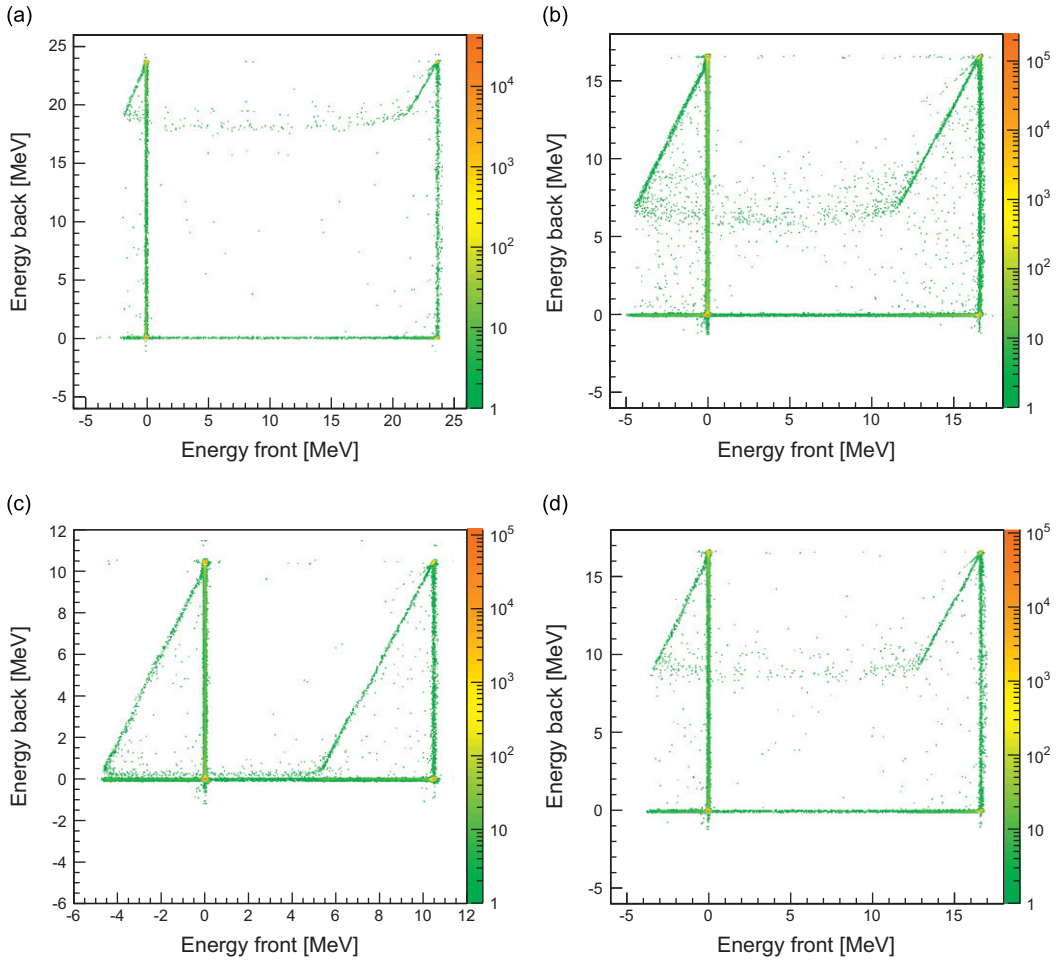

Fig. 7. Energy correlations between back strip 8 and front strip 7 and 8 for: (a) 1 FDV and ^{7}Li beam at 24 MeV; (b) 1 FDV and ^{7}Li beam at 17 MeV; (c) 1 FDV and ^{7}Li beam at 11 MeV; (d) 1.4 FDV and ^{7}Li beam at 17 MeV to be compared with (b).

fact that the incoming particles are crossing the front interstrip region.

In Fig. 7 the same front–back correlation plot is shown for different beam energies and for the two different bias. As one can see, the observed "energy defect" (ΔE in Fig. 6) on the back, for front interstrip events, decreases with increasing energy of the incoming particle and with the applied bias. This trend is confirmed also for the other energies investigated that are not shown in the present paper.

Fig. 8 shows, for comparison, the front–front correlations for the same energies and bias of the plots of Fig. 7. The systematic behavior of front–front correlations for the three different energies (a,b,c) of the ^{7}Li beam and the two different bias values (b,d) is shown. When the beam energy increases the amplitude of the opposite polarity signals decreases. The same effect is present when the bias applied to the detector increases; the trend is confirmed for all energies investigated. To our knowledge it is the first time that the dependence of the opposite polarity signals is observed as a function of the incident energy and of the applied bias.

3.3. Beam injected from the ohmic side

During the experiment, for each energy a third DSSSD 500 μm thick was irradiated from the ohmic side applying 1 FDV. In Figs. 9, 10 and 11 are shown, respectively, the plots for back–back correlations, front–front correlations and front–back correlations. They should be compared to Figs. 3, 4 and 6 obtained by irradiating the detector from the junction side. Looking at Fig. 10, we note that the behavior of the front interstrip, when particles are injected from the ohmic side, is similar to the back interstrip when particles are injected from the junction side (see Fig. 3). Analogously when particles are injected from the ohmic side the back interstrip (Fig. 9) behaves in a way similar to the front interstrip when particles are injected from the junction side (see Fig. 4) showing the presence of opposite polarity signals. It is

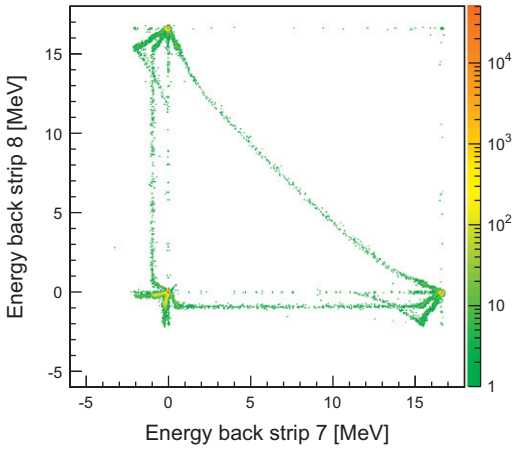

Fig. 9. Energy correlations between two adjacent back strips using a ^{7}Li beam at energy of 16.5 MeV injecting particles from the ohmic side.

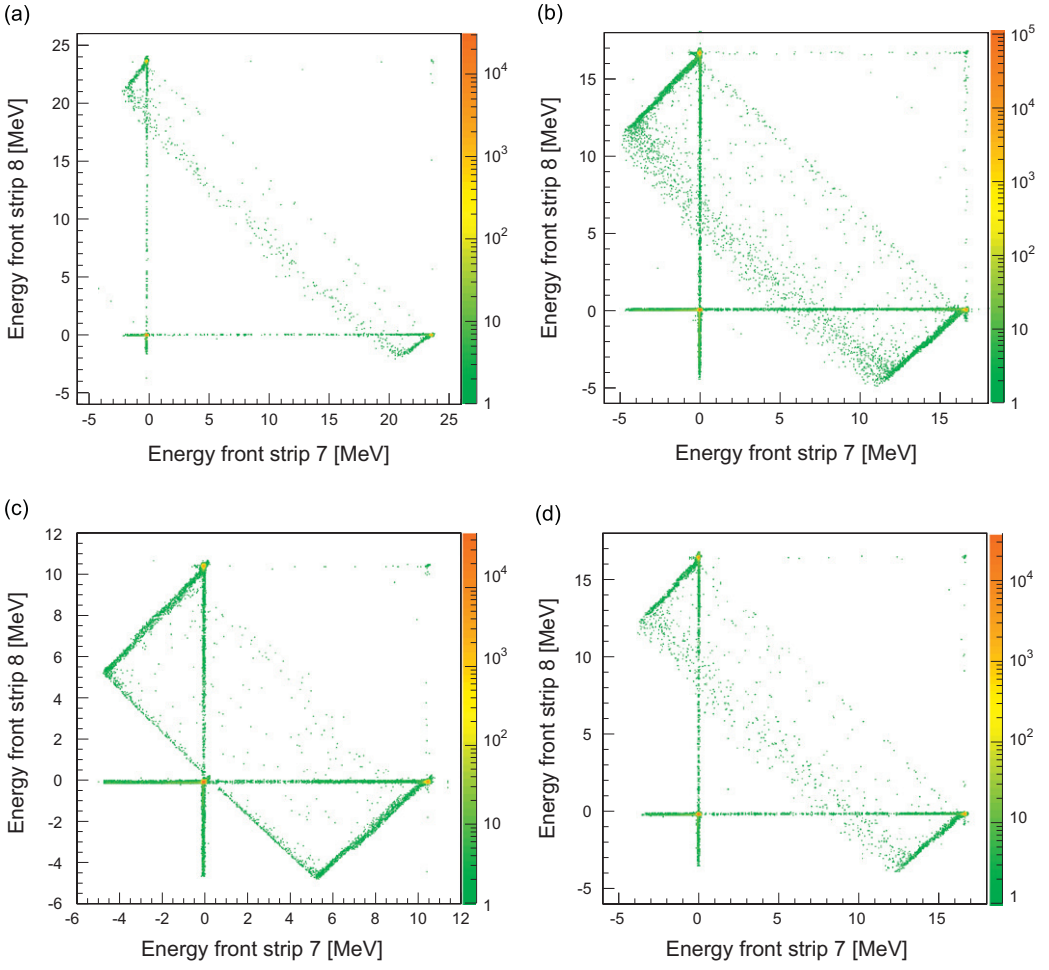

Fig. 8. Energy correlations between two front strips for: (a) 1 FDV and ^{7}Li beam at 24 MeV; (b) 1 FDV and ^{7}Li beam at 17 MeV; (c) 1 FDV and ^{7}Li beam at 11 MeV; (d) 1.4 FDV and ^{7}Li beam at 17 MeV to be compared with (b).

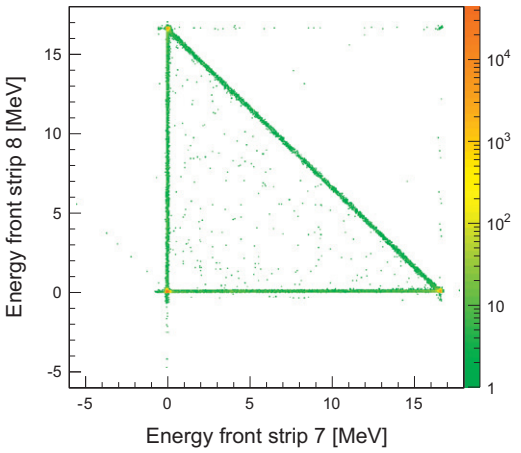

Fig. 10. Energy correlations between two adjacent front strips using a ^{7}Li beam at energy of 16.5 MeV injecting particles from the ohmic side.

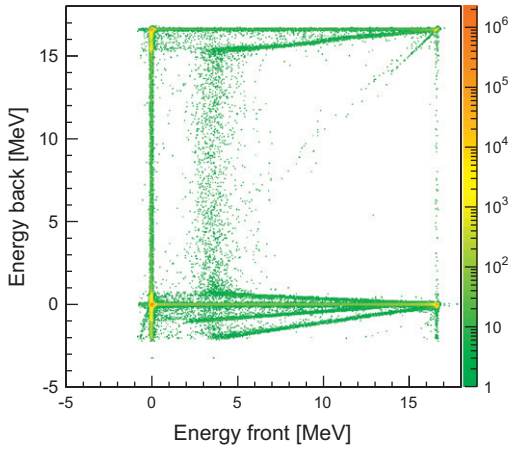

Fig. 11. Energy correlations between a front and all the back strips using a ^{7}Li beam at energy of 16.5 MeV injecting particles from the ohmic side.

true that Fig. 10 is essentially equal to Fig. 3, whereas Fig. 9 shows extra features with respect to Fig. 4. Some of these differences can be probably attributed to the fact that the detector irradiated from the ohmic side was biased with only 1 FDV. Therefore particles entering the detector from the ohmic side cross the region with extremely low electric field and this can generate a poor charge collection. Following these observations we can conclude that probably the difference in behavior between front and back interstrips, when particles enter the detector through the front, is not due (or at least not only due) to the different constructions of back and front sides. Opposite polarity signals seem to appear when particles cross the interstrip region, i.e. in front interstrip events when particles enter the detector from the front side and in back interstrip events when particles are injected from the back side. Therefore when DSSSDs are used in transparency opposite polarity signals will be probably present in both sides.

4. Discussion of the results

The presence of opposite polarity signals as well as the "energy defect" observed for back signals corresponding to the particles passing through the front interstrip region can be explained in the framework of the model proposed by Yorkston and collaborators [14]. In this model the front interstrip behavior is explained

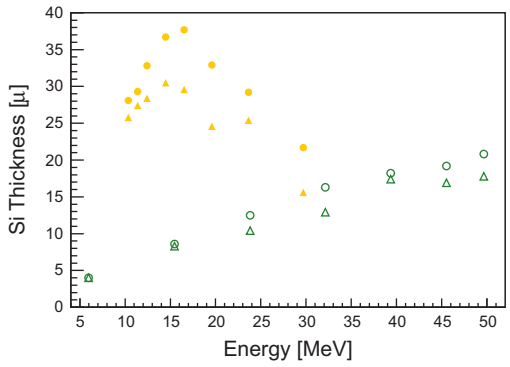

Fig. 12. Thickness of the anomalous filed region estimated from the energy defect measured in the back side. full (empty) symbols refer to Li (O) ions. Circles correspond to 1 FDV and triangle to 1.4 FDV.

invoking a local modification of the electric field due to the presence of the SiO_2 layer present in the interstrips.

According to the model, the amplitude of the opposite polarity signals (generated by induction phenomena) is related to the charges produced by the particles in the modified field region, and thus to the energy loss of the particles therein. The higher is the energy of the particle the lower is the amount of charge produced in the modified field region, and therefore the lower is the energy defect (and the lower is the amplitude of the opposite polarity signals). A rough estimation of the depth of the modified field region was inferred by using the incident energy of the particles and the "energy defect" observed in the back side for the front interstrip events. To this aim we calculated [19] the Si thickness in which a particle with initial energy E_{in} loses an amount of energy equal to the "energy defect". The results are shown in Fig. 12. Although it is not possible to get an unambiguous value for the depth of the modified field region, since it depends on the energy, on the ion species and on the bias, the estimated depth is anyhow between 5 and 40 μm. The interstrip effects, and in particular the presence of the opposite polarity signals, could be explained also in a different way, e.g. in the framework of the Shockley–Ramo theorem [20,21] or its generalization with the Gunn's theorem [22].

5. Selection procedures

We can conclude that, due to interstrip effects, there is a number of events where the energy measured is lower than the full energy one. Therefore, when using such detectors, one needs to apply a procedure that allows to select the correct full energy events rejecting the others. In addition, the efficiency associated with this full energy event selection has to be known. By using a set of mono-energetic beams, it is possible to properly test the selection procedure and to measure the associated efficiency for the full energy event detection. A common way to select the full energy events with DSSSDs is to compare the energy measured by the front side E_{front} with the one measured by the back side E_{back} by imposing $E_{front}=E_{back}$ within a given tolerance (in our case we have chosen 3σ). As an example, in Fig. 13 we compare the back energy spectrum with no conditions applied (empty histogram) with the same spectrum after applying the selection condition $E_{front}=E_{back}$ (full histogram). The same procedures applied to both front injected detectors for the other energies and different polarization voltages gave analogous results. One can clearly see that, after the selection, almost all events out of the FEP are removed. The fraction of events left out of the FEP, after applying the selection procedure, is about 2% which is compatible with

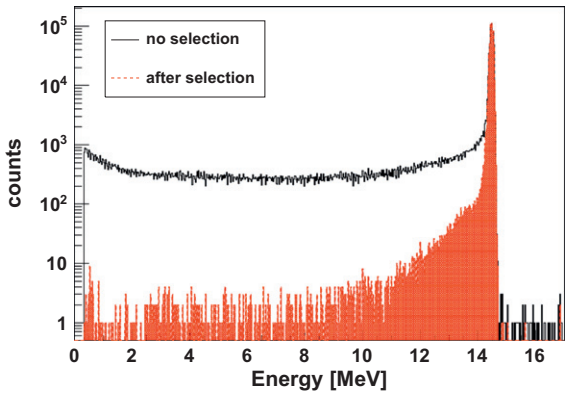

Fig. 13. Energy spectra for front strips before and after the selection $E_{front}=E_{back}$.

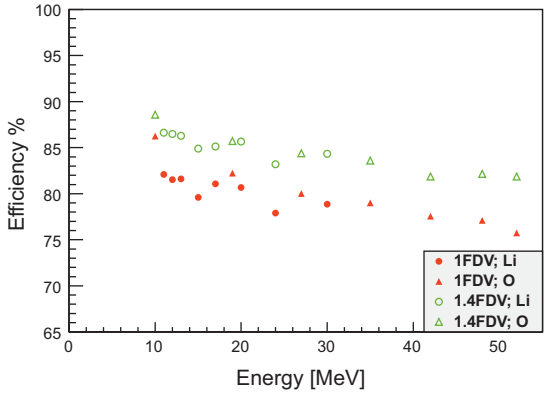

Fig. 14. Efficiency for the full energy reconstruction applying the condition $E_{front}=E_{back}$. The statistical error bars are smaller than the size of the symbols.

particles entering the detector with a degraded energy due, for instance, to scattering in the collimators.

In Fig. 14 we show the efficiency for full energy reconstruction when using the condition $E_{front}=E_{back}$ for different energies of the ^{7}Li and ^{16}O beams and for the two different used bias. As one can see, there is a non-negligible dependence of the efficiency for full energy selection on the energy and ion species, as well as on the bias supplied to the detector: the higher is the bias the lower is the number of interstrip events.

We remind that, as shown before (as well as in Refs. [14,15]), the charge generated by a particle whose trajectory crosses a back interstrip is collected by the two adjacent strips with no loss of charge. Therefore, in order to recover the back interstrip events, one can sum the pulses of the two adjacent strips and can use the following alternative methods to select events. If no adjacent back strips give coincident signals above the threshold, the back signal is compared with the front one and the usual $E_{front}=E_{back}$ condition can be used. If there are two adjacent back strips that give a signal above the threshold, the two corresponding energies are summed and then compared with the energy measured by the front strips. The efficiency for full energy reconstruction obtained by using this method is shown in Fig. 15 as a function of the ion energy and polarization voltage.

As one can see by comparing Figs. 14 and 15, the efficiency is significantly increased and its dependence on the incident energy and on the bias is removed. The obtained efficiency, around 94%, is however still lower than the geometrical one which is around 97%. If the detector is used in transparency mode, according to the results shown in Figs. 10 and 11, and discussed in Section 3.3, opposite polarity signals are expected to appear also in the back side. In this case recovering back side interstrip events is not

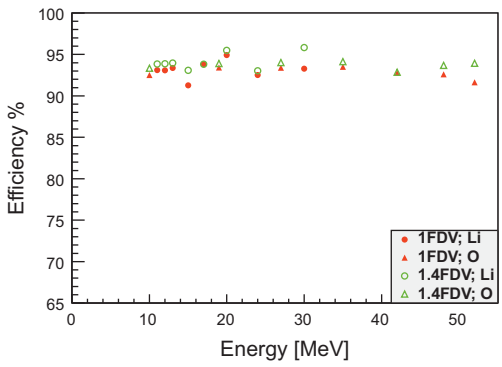

Fig. 15. Efficiency for full energy reconstruction obtained by imposing the condition $E_{front}=E_{back}$ after recovering the back interstrip events. The statistical error bars are smaller than the size of the symbols. See text for details.

possible and the efficiency for the full energy reconstruction will be lower.

All the above-mentioned tests were performed with the detectors placed at 0° (i.e. direction of the beam perpendicular to the detector). The number of interstrip events could increase if the angle of incidence is different than zero. We underline that this procedure was applied with a very low rate, around 100 pps, corresponding to few tens of particles per second in the strip with the largest counting rate. The probability that two particles hit two adjacent strips within the same acquisition gate was negligible.

6. Summary and conclusions

We performed a characterization of Double Sided Silicon Strip Detectors with the aim to carry out a systematic study of the interstrip effects on the energy measurement of charged particles. The study was performed with ^{7}Li and ^{16}O beams in the energy range 6–50 MeV. The used charged particles were heavier than those used in other tests reported in literature (H, ^{4}He) [14,15].

The effect of the applied bias voltage was also investigated. For the first time we studied the efficiency for full energy detection, the number of interstrip events and the amplitude of the opposite polarity signals varying the energy of the incident particles and the bias applied to the detector. The performed tests showed, for the first time to our knowledge, that when particles are injected from the ohmic side, opposite polarity signals for interstrip events are observed in the back strips, whereas they disappear in the front strips. Therefore, the different behaviors of the front and back interstrips do not seem to be due to their different structures, and one could expect that opposite polarity signals are generated on both faces when the detectors are used in transparency.

The use of mono-energetic beams allowed us to test the event selection procedure and to extract the efficiency for the full energy reconstruction. Our data show that for particles injected from the front side and stopping inside the detector, the back interstrip events can be easily recovered by summing the signals coming in coincidence from two adjacent strips. On the contrary front interstrip events, that generate opposite polarity signals, cannot be recovered. We found that the fraction of events measured with the correct energy, both for the front and the back sides and without any reconstruction, is lower than the value of 94% which one can estimate from geometrical considerations taking into account the active surface on both faces. This means that the effective width of the interstrip region is larger than the geometrical one (100 μm). Moreover, we found that the

experimental efficiency depends on the incident energy, ion species and applied bias. Using the proposed procedure described here we can maximize the efficiency for full energy reconstruction and remove its dependence on the energy, ion species and applied bias.

References

[1] A. Di Pietro, V. Scuderi, A.M. Moro, L. Acosta, F. Amorini, M.J.G. Borge, P. Figuera, M. Fisichella, L.M. Fraile, J. Gomez-Camacho, H. Jeppesen, M. Lattuada, I. Martel, M. Milin, A. Musumarra, M. Papa, M.G. Pellegriti, F. Perez-Bernal, R. Raabe, G. Randisi, F. Rizzo, G. Scalia, O. Tengblad, D. Torresi, A.M. Vidal, D. Voulot, F. Wenander, M. Zadro, Physical Review C 85 (2012) 054607.

[2] L. Acosta, A.M. Sanchez-Benítez, M.E. Gómez, I. Martel, F. Pérez-Bernal, F. Pizarro, J. Rodríguez-Quintero, K. Rusek, M.A.G. Alvarez, M.V. Andrés, J.M. Espino, J.P. Fernández-García, J. Gómez-Camacho, A.M. Moro, C. Angulo, J. Cabrera, E. Casarejos, P. Demaret, M.J.G. Borge, D. Escrig, O. Tengblad, S. Cherubini, P. Figuera, M. Gulino, M. Freer, C. Metelko, V. Ziman, R. Raabe, I. Mukha, D. Smirnov, O.R. Kakuee, J. Rahighi, Physical Review C 84 (2011) 044604.

[3] A. Di Pietro, G. Randisi, V. Scuderi, L. Acosta, F. Amorini, M.J.G. Borge, P. Figuera, M. Fisichella, L.M. Fraile, J. Gomez-Camacho, H. Jeppesen, M. Lattuada, I. Martel, M. Milin, A. Musumarra, M. Papa, M.G. Pellegriti, F. Perez-Bernal, R. Raabe, F. Rizzo, D. Santonocito, G. Scalia, O. Tengblad, D. Torresi, A.M. Vidal, D. Voulot, F. Wenander, M. Zadro, Physical Review Letters 105 (2010) 022701.

[4] A. Di Pietro, P. Figuera, F. Amorini, C. Angulo, G. Cardella, S. Cherubini, T. Davinson, D. Leanza, J. Lu, H. Mahmud, M. Milin, A. Musumarra, A. Ninane, M. Papa, M.G. Pellegriti, R. Raabe, F. Rizzo, C. Ruiz, A.C. Shotter, N. SoićS. Tudisco, L. Weissman, Physical Review C 69 (2004) 044613.

[5] A. Di Pietro, F. Amorini, W. Bradfield-Smith, G. Cardella, T. Davinson, P. Figuera, W. Galster, R. Irvine, P. Leleux, J. Mackenzie, A. Musumarra, R. Neal, A. Ninane, G. Pappalardo, F. Rizzo, A.C. Shotter, C. Sükösd, S. Tudisco, Physical Review C 59 (1999) 1185.

[6] M. Milin, S. Cherubini, T. Davinson, A.D. Pietro, P. Figuera, . Miljanić, A. Musumarra, A. Ninane, A. Ostrowski, M. Pellegriti, A. Shotter, N. Soićs, C. Spitaleri, M. Zadro, Nuclear Physics A 730 (2004) 285.

[7] V.Z. Goldberg, G.V. Rogachev, W.H. Trzaska, J.J. Kolata, A. Andreyev, C. Angulo, M.J.G. Borge, S. Cherubini, G. Chubarian, G. Crowley, P. Van Duppen, M. Gorska, M. Gulino, M. Huyse, P. Jesinger, K.-M. Källman, M. Lattuada, T. Lönnroth, M. Mutterer, R. Raabe, S. Romano, M.V. Rozhkov, B.B. Skorodumov, C. Spitaleri, O. Tengblad, A. Tumino, Physical Review C 69 (2004) 024602.

[8] K.P. Artemov, O. Belyanin, A. Vetoshkin, R. Wolski, M. Golovkov, V. Goldberg, M. Madeja, V. Pankratov, I. Serikov, V. Timofeev, V. Shadrin, J. Szmider, Soviet Journal of Nuclear Physics 52 (1990) 406.

[9] D. Torresi, M. Lattuada, A. Musumarra, M. Pellegriti, M. Rovituso, G. Scalia, E. Strano, L. Cosentino, A. Di Pietro, P. Figuera, C. Maiolino, D. Santonocito, C. Ducoin, M. Papa, M. Fisichella, T. Lonnroth, V. Scuderi, M. Zadro, International Journal of Modern Physics E 20 (04) (2011) 1026.

[10] M. Freer, N.I. Ashwood, N. Curtis, A. Di Pietro, P. Figuera, M. Fisichella, L. Grassi, D. Jelavić Malenica, T. Kokalova, M. Koncul, T. Mijatović, M. Milin, L. Prepolec, V. Scuderi, N. Skukan, N. Soić, S. Szilner, V. Tokić, D. Torresi, C. Wheldon, Physical Review C 84 (2011) 034317.

[11] A.I. Morales, J. Benlliure, J. Agramunt, A. Algora, N. Alkhomashi, H. Álvarez-Pol, P. Boutachkov, A.M. Bruce, L.S. Cáceres, E. Casarejos, A.M. Denis Bacelar, P. Doornenbal, D. Dragosavac, G. Farrelly, A. Gadea, W. Gelletly, J. Gerl, M. Górska, J. Grebosz, I. Kojouharov, F. Molina, D. Pérez-Loureiro, S. Pietri, Z. Podolyák, P.H. Regan, B. Rubio, H. Shaffner, S.J. Steer, S. Tashenov, S. Verma, H.J. Wollersheim, Physical Review C 84 (2011) 011601.

[12] M.M. Rajabali, R. Grzywacz, S.N. Liddick, C. Mazzocchi, J.C. Batchelder, T. Baumann, C.R. Bingham, I.G. Darby, T.N. Ginter, S.V. Ilyushkin, M. Karny, W. Królas, P.F. Mantica, K. Miernik, M. Pfützner, K.P. Rykaczewski, D. Weisshaar, J.A. Winger, Physical Review C 85 (2012) 034326.

[13] S. Nishimura, Z. Li, H. Watanabe, K. Yoshinaga, T. Sumikama, T. Tachibana, K. Yamaguchi, M. Kurata-Nishimura, G. Lorusso, Y. Miyashita, A. Odahara, H. Baba, J.S. Berryman, N. Blasi, A. Bracco, F. Camera, J. Chiba, P. Doornenbal, S. Go, T. Hashimoto, S. Hayakawa, C. Hinke, E. Ideguchi, T. Isobe, Y. Ito, D.G. Jenkins, Y. Kawada, N. Kobayashi, Y. Kondo, R. Krücken, S. Kubono, T. Nakano, H.J. Ong, S. Ota, Z. Podolyák, H. Sakurai, H. Scheit, K. Steiger, D. Steppenbeck, K. Sugimoto, S. Takano, A. Takashima, K. Tajiri, T. Teranishi, Y. Wakabayashi, P.M. Walker, O. Wieland, H. Yamaguchi, Physical Review Letters 106 (2011) 052502.

[14] J. Yorkston, A. Shotter, D. Syme, G. Huxtable, Nuclear Instruments and Methods in Physics Research Section A: Accelerators, Spectrometers, Detectors and Associated Equipment 262 (2–3) (1987) 353.

[15] Y. Blumenfeld, F. Auger, J. Sauvestre, F. Maréchal, S. Ottini, N. Alamanos, A. Barbier, D. Beaumel, B. Bonnereau, D. Charlet, J. Clavelin, P. Courtat, P. Delbourgo-Salvador, R. Douet, M. Engrand, T. Ethvignot, A. Gillibert, E. Khan, V. Lapoux, A. Lagoyannis, L. Lavergne, S. Lebon, P. Lelong, A. Lesage, V. Ven, I. Lhenry, J. Martin, A. Musumarra, S. Pita, L. Petizon, E. Pollacco, J. Pouthas, A. Richard, D. Rougier, D. Santonocito, J. Scarpaci, J. Sida, C. Soulet, J. Stutzmann, T. Suomijärvi, M. Szmigiel, P. Volkov, G. Voltolini, Nuclear Instruments and Methods in Physics Research Section A: Accelerators, Spectrometers, Detectors and Associated Equipment 421 (3) (1999) 471.

[16] S. Takeda, S. Watanabe, T. Tanaka, K. Nakazawa, T. Takahashi, Y. Fukazawa, H. Yasuda, H. Tajima, Y. Kuroda, M. Onishi, K. Genba, Nuclear Instruments and Methods in Physics Research Section A: Accelerators Spectrometers Detectors and Associated Equipment 579 (2) (2007) 859.

[17] V. Eremin, J. Bohm, S. Roe, G. Ruggiero, P. Weilhammer, Nuclear Instruments and Methods in Physics Research Section A: Accelerators, Spectrometers, Detectors and Associated Equipment 500 (1–3) (2003) 121.

[18] C. Wrede, A. Hussein, J.G. Rogers, J. D'Auria, Nuclear Instruments and Methods in Physics Research Section B: Beam Interactions with Materials and Atoms 204 (2003) 619.

[19] O. Tarasov, D. Bazin, 〈http://groups.nscl.msu.edu/lise/lise.html〉.

[20] G. Cavalleri, G. Fabri, E. Gatti, V. Svelto, Nuclear Instruments and Methods 21 (1963) 177.

[21] G. Cavalleri, E. Gatti, G. Fabri, V. Svelto, Nuclear Instruments and Methods 92 (1) (1971) 137.

[22] E. Vittone, Nuclear Instruments and Methods in Physics Research Section B: Beam Interactions with Materials and Atoms 219–220 (2004) 1043.